Journal of Earth Science, Vol. 28, No. 2, p. 249–264, April 2017 *ISSN 1674-487X*
Printed in China
DOI: 10.1007/s12583-016-0912-2

Geochronology, Geochemistry and Tectonic Significance of the Early Carboniferous Gabbro and Diorite Plutons in West Ujimqin, Inner Mongolia

Shiwei Ma[1], **Changfeng Liu**[2], **ZhiqinXu**[1], **Zhiguang Zhou***[4], **Jinyuan Dong**[3], **Hongying Li**[4]
1. *Institute of Geology*, *Chinese Academy of Geological Sciences*, *Laboratory for Continental Tectonics and Dynamics*, *Beijing* 100037, *China*
2. *Institute of Geology Survey*, *China University of Geosciences*, *Beijing* 100083, *China*
3. *Key Laboratory of Active Tectonics and Volcano*, *Institute of Geology*, *China Earthquake Administration*, *Beijing* 100029, *China*
4. *School of Earth Sciences and Resources*, *China University of Geosciences*, *Beijing* 100083, *China*
Shiwei Ma: http://orcid.org/0000-0002-4775-9829; Zhiguang Zhou: http://orcid.org/0000-0001-8925-4725

ABSTRACT: Early Carboniferous gabbros and diorites are distributed in West Ujimqin, Inner Mongolia. The LA-ICP-MS zircon U-Pb ages of the gabbro and diorite samples are 321±2 Ma (MSWD=0.65) and 319.4±1.5 Ma (MSWD=0.42), respectively. In addition, new geochemistry data from three gabbro and three diorite samples are presented. All six samples show high Al_2O_3 contents but low-TiO_2 contents, belonging to tholeiitic and calc-alkali basalt series. All of the samples have similar chondrite normalized REE patterns characterized by moderate depletion in LREE similar to normal middle oceanic ridge basalt (MORB). The MORB and PM-normalized trace element patterns show the enrichment in large ion lithophile elements (LILE, e.g., Rb, Ba and Sr), depletion in high field strength elements (HFSE) and distinctly negative Nb and Ta anomalies similar to volcanic arc basalt. Furthermore, as shown in the correlation plots of La/Ba vs. La/Nb, Ba/La vs. Ce/Pb, Th/La vs. Ce/Pb, Nb/La vs. Ba/Rb, and Nb/Y vs. La/Yb, the magma source has undergone contamination and metasomatism from the subduction fluid. According to the Zr/Nb, La/Nb, and La/Ta ratios and the Nb/Y vs. Zr/Y and Sm/Yb vs. La/Sm diagrams, the magma was derived from shallow depleted lithospheric mantle and formed by moderate (5%–20%) partial melting of spinel lherzolites. Tectonic setting discrimination diagrams reveal that the gabbros and diorites display both characteristics of MORB and volcanic arc basalt, which is consistent with their geochemical characteristics. On the basis of the geochemical features of these samples, combined with regional geological data and many previous researches in the study area, the Early Carboniferous gabbros and diorites of West Ujimqin are suggested to be formed in an intensely extensional rift setting, and a limited immature ocean basin probably formed after subsequent development.

KEY WORDS: zircon U-Pb age, geochemistry, extensional setting, Early Carboniferous, West Ujimqin.

0 INTRODUCTION

The Central Asian Orogenic Belt (CAOB) is a wide accretionary orogeny of the Phanerozoic Era (Xiao et al., 2015a, 2003; Liu et al., 2015, 2014, 2012; Xu et al., 2014; Li et al., 2013, 2012a, b; 2006; Jian et al., 2012; Jahn et al., 2009, 2004, 2001, 2000a, b, c; Hong et al., 2003a; Badarch et al., 2002; Sengör et al., 1993), and also is a famous metallogenic province (Wu et al., 2015, 2014; Xiao et al., 2009, 2008; Zhai et al., 2002). The tectonic evolution of the CAOB has been a hotspot of geological research during recent years. However, the detailed accretionary process remains controversial among the international academic communities (Liu et al., 2015, 2014; Shao et al., 2014, 1991; Windley et al., 2007; Xiao et al., 2003; Sengör et al., 1996; Tang et al., 1993, 1990). The eastern CAOB extends across Inner Mongolia and Northeast China and is named the Xing'an Mongolia orogenic belt (XMOB) (Xu et al., 2014; Shao, 1991; Ren et al., 1980). The XMOB experienced a long-term subduction of the Paleo-Asian Ocean, and accretion led to the formation island arcs, forearc or back-arc basins, ophiolitic belts, and microcontinents from the Neoproterozoic to Late Paleozoic (Xiao et al., 2015a, b, 2014a, b, 2013, 2012; Jian et al., 2010, 2008; Sengör et al., 1993). Despite those studies, there has been a debate in terms of the Late Paleozoic tectonic evolution in Inner Mongolia, especially regarding the precise closing time of the Paleo-Asian Ocean.

*Corresponding author. zhouzhg@cugb.edu.cn

Manuscript received October 18, 2015.
Manuscript accepted April 16, 2016.

Ma, S. W., Liu, C. F., Xu, Z. Q., et al., 2017. Geochronology, Geochemistry, and Tectonic Significance of the Early Carboniferous Gabbro and Diorite from the West Ujimqin, Inner Mongolia. *Journal of Earth Science*, 28(2): 249–264. doi: 10.1007s12583-016-0912-2. http://en.earth-science.net

Some scholars held the opinion that the Paleo-Asian Ocean was closed in the Devonian (Zhu et al., 2004). Some scholars agreed with the viewpoint that the closure occurred in the Early Carboniferous (Shao et al., 2014, 1991; Cao et al., 1986). Meanwhile, other scholars believed that the closure of the Paleo-Asian Ocean occurred during the Permian (Xiao et al., 2015, 2003; Li et al., 2006; Miao et al., 2006; Chen et al., 2001; Sengor et al., 1993).

West Ujimqin is located at the central Inner Mongolia, and belongs to the XMOB. Detailed structural and stratigraphic investigations are challenging in this region, and the tectonic setting of the West Ujimqin has been a source of scientific controversy. Voluminous Paleozoic–Early Mesozoic magmatism occurred in this region and may provide information regarding the tectonic evolution and constraints on the middle part of the XMOB or CAOB (Li et al., 2016; Liu et al., 2016; Li et al., 2015, 2013, 2012b; Dong., 2014; Bai., 2013; Liu et al., 2009; Bao et al., 2007, 2006; Su et al., 1996). However, the petrogenesis and tectonic settings of Early Carboniferous magmatism are poorly constrained due to the scarcity of geochemical and geochronologic data in this region. Through a regional geological survey at 1 : 50 000 scale, we first discovered the Early Carboniferous gabbro. Owing to this contribution, we present new zircon LA-ICP-MS U-Pb dating and geochemical data for the Early Carboniferous gabbros and diorites from West Ujimqin, to better discuss the petrogenesis and the Late Paleozoic tectonic evolution.

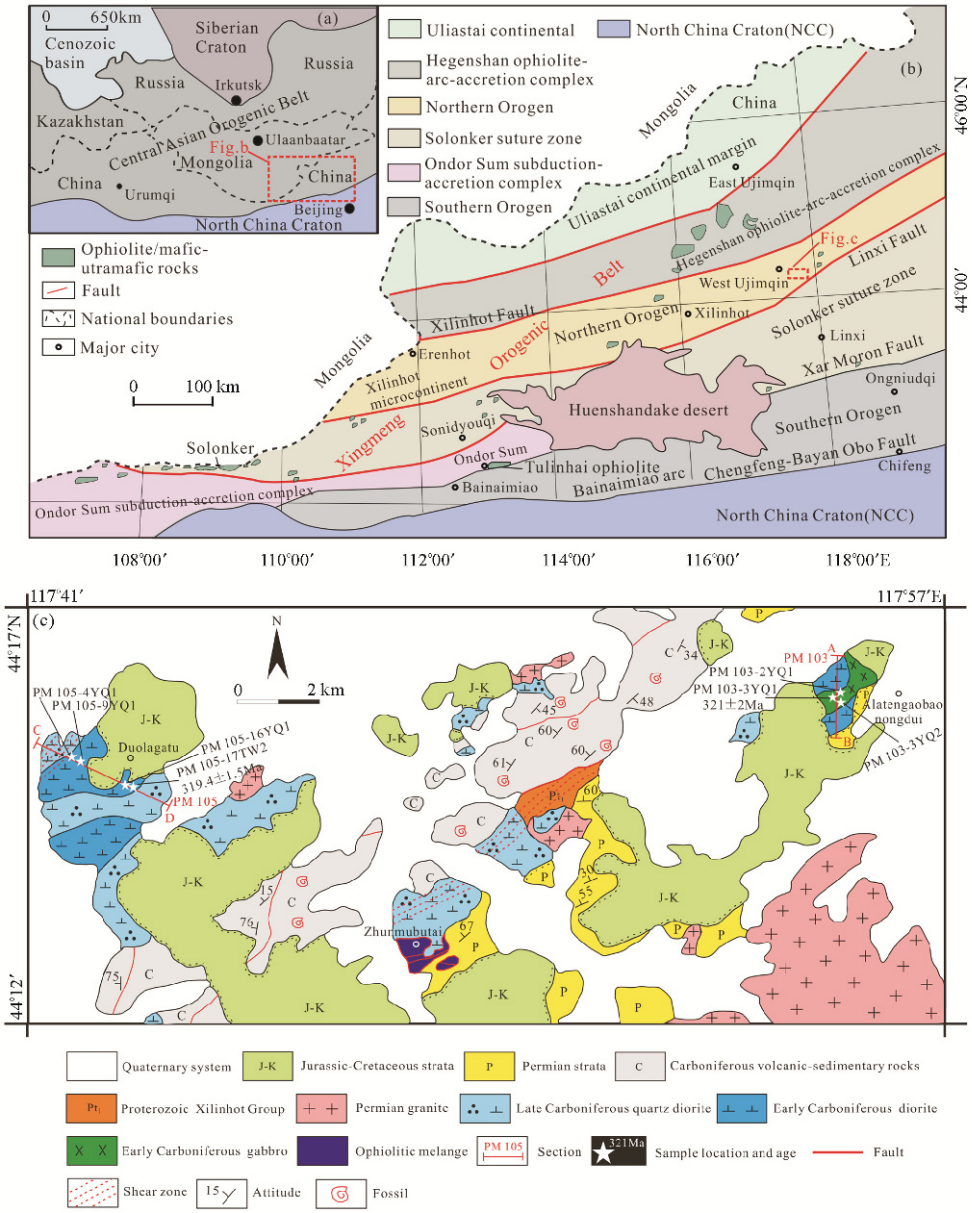

Figure 1. Sketch maps of Inner Mongolia, the Xingmeng orogenic belt, and the study area. (a) Geotectonic location of Inner Mongolia (modified from Jian et al., 2008). (b) Geological map of the Xingmeng orogenic belt, modified from Jian et al. (2008) based on our own observations showing the Solonker suturezone separating the Northern and Southern Paleozoic orogens. (c) Geological map of the study area, southern West Ujimqin (modified from 1 : 50 000 geological maps of Houtoumiao and Alatengaobaonongdui).

1 GEOLOGICAL SETTING AND SAMPLING AND PETROGRAPHY

1.1 Geological Setting

West Ujimqin is situated, tectonically, in the Northern Orogen in the middle of the XMOB (Fig. 1b). It is a critical area to reveal the tectonic evolution of the Paleo-Asian Ocean and XMOB. The most ancient strata in the study area are Xilin Hot Group (BGMRN, 1991). Strata overlying the Xilin Hot Group include Carboniferous volcanic-sedimentary rocks, Permian strata and Jurassic–Cretaceous strata which are all deposits of continental or marine-terrigenous facies. The magmatic activities were frequent during Late Paleozoic. A newly discovered ophiolitic mélange outcrops at Zhunmubutai District show that Early Carboniferous intrusive rocks are composed of gabbro and diorite. Late Carboniferous quartz diorite intrudes into ophiolitic mélange, Early Carboniferous diorite and Carboniferous volcanic-sedimentary rocks. Permian intrusions are dominated by granite.

The gabbro and diorite plutons of this study are mainly distributed in Alatengaobaonongdui and Houtoumiao which located in the south of West Ujimqin (Fig. 1c). The plutons are poorly exposed, with outcrops that are cracked but relatively fresh. We have constructed cross sections across the gabbro and diorite plutons (Figs. 1c and 2). The Section PM103 (Fig. 2a) reveals that the diorite intruded the gabbro. And the Section PM105 (Fig. 2b) shows that the diorite is intruded by Late Carboniferous quartz diorite. The gabbro and diorite are unconformably overlain by Permian and Jurassic–Cretaceous strata.

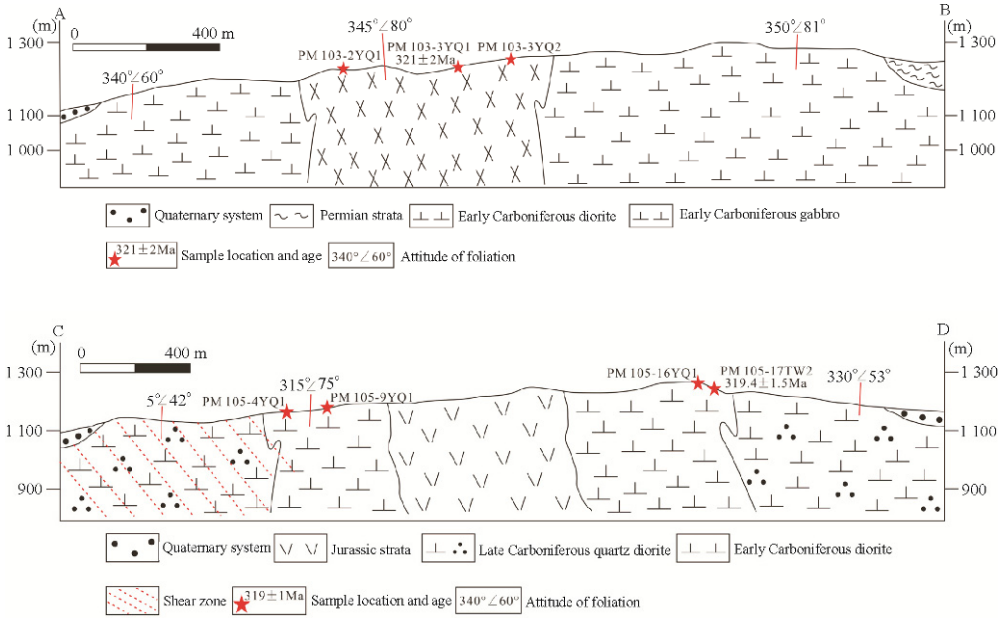

Figure 2. Cross-sections of the gabbro and the diorite in this study (the section locations are in Fig. 1).

1.2 Sampling and Petrography

Fresh gabbros and diorites were sampled from the southern West Ujimqin. In this paper, we present geochemical data of three gabbroic and three dioriteic samples. Additionally, we collect two geochronologic data for gabbro and diorite samples. The sample locations are shown in Fig. 1c.

The Early Carboniferous gabbro plutons were mapped for the first time through regional geological survey in Alatengaobaonongdui which covers an area of 4 km^2 at 1 : 50 000 scale. The gabbros mainly exhibit gabbroic texture and massive structure. They have three types of granular textures in the field, i.e., fine-grained, coarse-to medium-grained, and coarse-grained, from the rim to the core of the pluton (Fig. 3a and 3b). The gabbros are comprised of plagioclase (~60 vol.%), pyroxene(~30 vol.%), hornblende (~8 vol.%), and a few accessory minerals such as zircon, titanomagnetite and apatite (Figs. 3e and 3f). Some samples have underwent slight alteration, for example, zoisitization and sericitization occured in plagioclase grains, amphibolization presented in some pyroxene grains, and actinolitization exists in some hornblende grains.

The Early Carboniferous diorite exposed in Houtoumiao village is a small rock stock of about 5 km^2. The diorite stock shows fine-grained texture and massive structure. In some locations, the fine-grained diorites experienced weak mylonitization (Figs. 3c and 3d). The diorites are consisted of plagioclase (~55 vol.%), hornblende (~40 vol.%), quartz (~2 vol.%), biotite (~2 vol.%), and various accessory minerals, such as zircon, sphene and magnetite (Figs. 3g and 3h). Some mineral grains have undergone slight alteration, e.g., sericitization occurred in plagioclase grains, epidotization exists in some hornblende grains, and chloritization presented in biotite grains.

2 ANALYTICAL METHODS

Zircons were selected for U-Pb dating at the laboratory of the Hebei Institute of Regional Geology and Mineral Resources Survey. Zircons for U-Pb analysis were separated by conventional magnetic and density techniques to concentrate non-magnetic, heavy fractions. Transmitted and reflected light micrographs and cathodoluminescence (CL) images were used

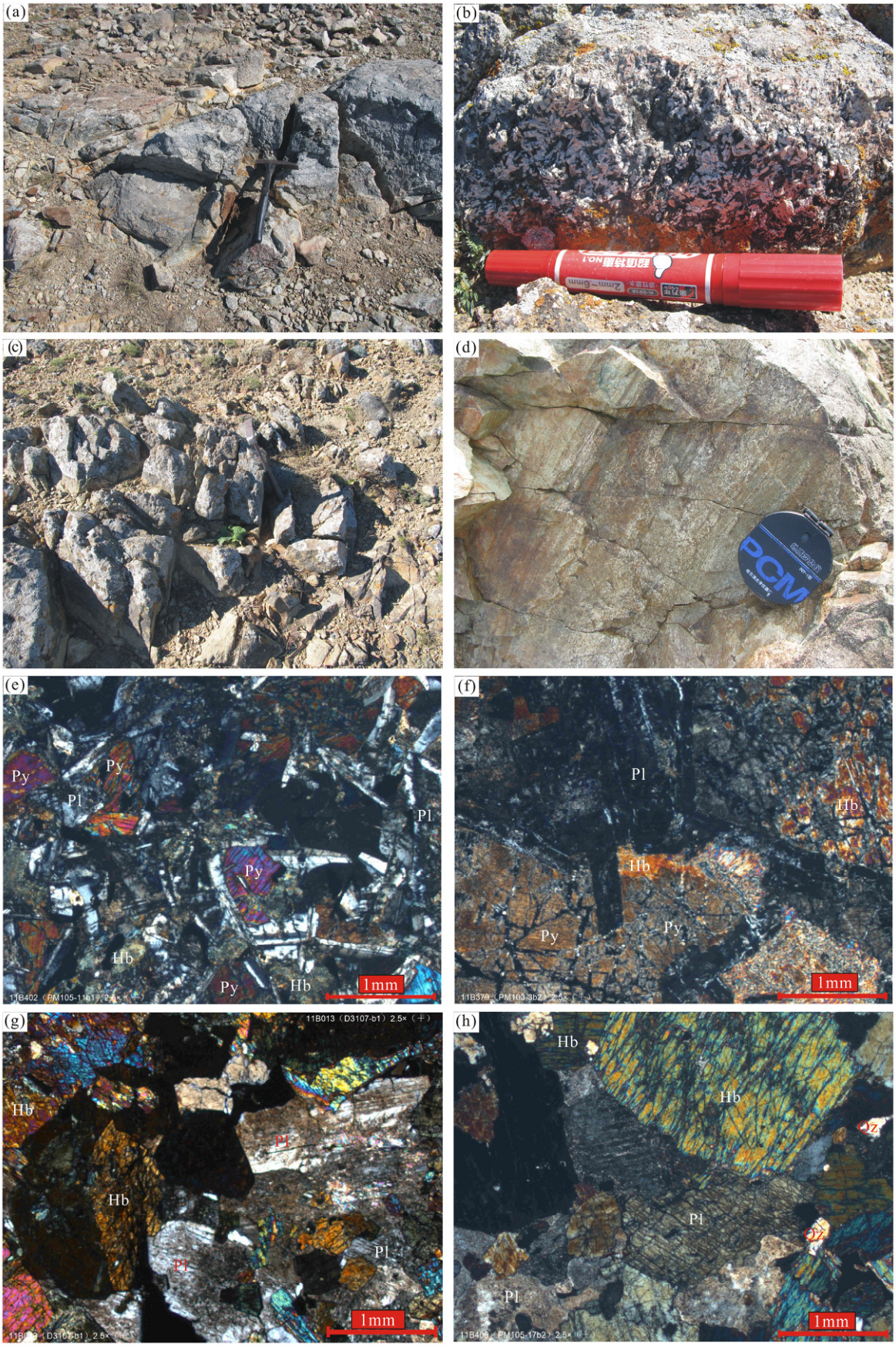

Figure 3. Representative field photos and photomicrographs. (a & b) gabbros; (c & d), diorites; (e & f) photomicrographs of gabbros; (g & h) photomicrographs of diorites. Hb. Hornblende; Pl. Plagioclase; Py. Pyroxene.

to guide the U-Th-Pb isotope analysis. The CL study was conducted at Beijing Zirconium Technology Limited Company. Zircon U-Pb isotopic compositions were analyzed at the laboratory of the Tianjin Geological Survey Center using LA-ICP-MS. The specific experimental principles and data analytical procedures were modeled after Li H K (2010, 2009).

All samples were crushed and powered in an agate mortar to an average size of less than 200 μm and then saved in clean plastic bags. Contamination from other samples was avoided, and the utensils used for grinding were kept the same for each sample to guarantee their representativeness. Major elements were analyzed by XRF at the laboratory of the Hebei Institute of Regional Geology and Mineral Resources Survey, with an analytical uncertainty of less than 5%. Trace elements and rare earth elements were determined by ICP-MS at the laboratory of the Hebei Institute of Regional Geology and Mineral Resources Survey, with analytical precision better than 10%.

3 RESULTS

3.1 Zircon U-Pb Geochronology

The representative zircon CL images from gabbro and diorite samples are shown in Figs. 4a and 4b, respectively. The LA-ICP-MS zircon U-Pb analytical data are given in tables 1 and 2, and the results are plotted on the Wetherill-type Concordia diagrams (Figs. 5a and 5b).

The coordinates of the gabbro sample (PM103-3TW1) are 44°15′59″N, 117°54′55″E. The zircons are colorless to dark brown, subhedral to euhedral, short columnar to long columnar and with length/width ratios between 2 : 1 and 3 : 1 (Fig. 4a). Most of the zircons show densely oscillatory zoning, indicating an igneous origin (Pidgeon, 1996; Hancher and Miller, 1993) and a high temperature environment of formation (Wu and Zheng, 2004). The U concentrations of zircons vary from 36 to 528 ppm and the Th/U ratios are between 0.30 and 1.05, which also suggests the magmatic origin (Koschek, 1993). Thirteen analyses define an age population with a weighted mean $^{206}Pb/^{238}U$ age of 321±2.0 Ma (MSWD=0.65) (Fig. 5a), which is interpreted as the best estimate of the crystallization age for the gabbro (Fig. 5b).

The diorite sample (PM105-17TW2) is located at 44°15′59″N, 117°54′55″E. The zircons are light brown, irregularly shaped, and granular, with a few arranged in short columns. Most of the zircons lack typical oscillatory zoning (Fig. 4b). The U concentrations of zircons range from 67 ppm to 1 455 ppm, and the Th/U ratios vary from 0.12 to 0.67, indicating of a magmatic origin (Koschek, 1993). Sixteen analyses define an age population with a weighted mean $^{206}Pb/^{238}U$ age of 319.4±1.5 Ma (MSWD=0.42), which is considered as the intrusion age of the diorite (Fig. 5b).

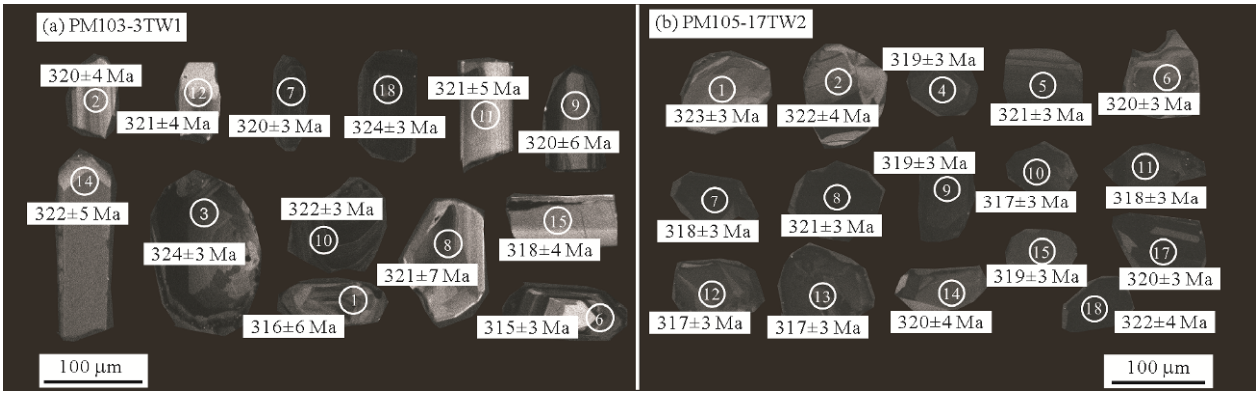

Figure 4. CL images for analyzed zircon grains from the gabbro (a) and diorite (b). Circles indicate the locations of analyzed sites.

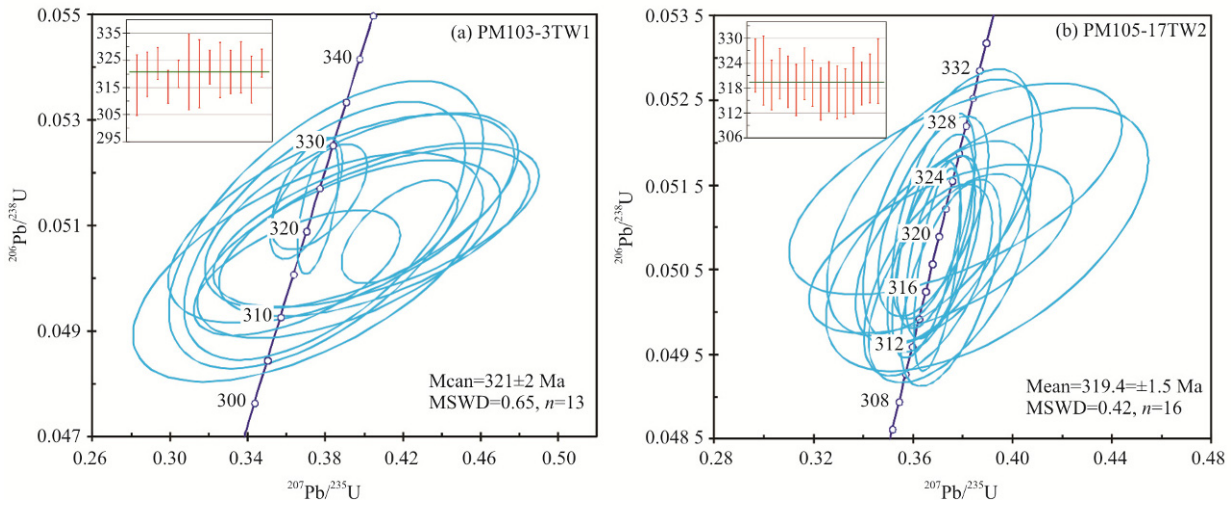

Figure 5. Concordia diagrams for analyzed zircon grains from the gabbro (a) and diorite (b).

Table 1 Analytical U-Pb zircon data of gabbros (PM103-3TW1) from West Ujimqin

Spot	Content (ppm)		$^{232}Th/^{238}U$	Isotope ratios						Apparent ages (Ma)			
	Pb	U		$^{206}Pb/^{238}U$	1σ	$^{207}Pb/^{235}U$	1σ	$^{207}Pb/^{206}Pb$	1σ	$^{206}Pb/^{238}U$	1σ	$^{207}Pb/^{235}U$	1σ
1	6	108	0.407 4	0.050 2	0.000 9	0.371 3	0.036 8	0.053 6	0.003 7	316	6	321	32
2	5	81	0.297 5	0.050 9	0.000 7	0.405 4	0.032 7	0.057 8	0.004 4	320	4	346	28
3	13	253	0.349 5	0.051 5	0.000 5	0.370 4	0.007 6	0.052 1	0.001 1	324	3	320	7
4	4	162	0.473 6	0.021 7	0.000 3	0.148 4	0.013 8	0.049 5	0.004 7	139	2	141	13
5	15	329	0.614 5	0.043 9	0.000 4	0.321 2	0.005 7	0.053 1	0.000 9	277	3	283	5
6	10	177	1.053 5	0.050 1	0.000 5	0.365 6	0.021 7	0.052 9	0.003 1	315	3	316	19
7	28	467	0.834 0	0.050 9	0.000 4	0.418 3	0.012 2	0.059 6	0.001 5	320	3	355	10
8	5	80	0.591 2	0.051 0	0.001 1	0.380 7	0.033 1	0.054 1	0.004 7	321	7	328	28
9	6	98	0.415 5	0.050 9	0.001 0	0.379 8	0.029 6	0.054 1	0.004 1	320	6	327	25
10	29	528	0.681 0	0.051 3	0.000 5	0.376 2	0.004 4	0.053 2	0.000 6	322	3	324	4
11	2	36	0.608 9	0.051 1	0.000 8	0.388 2	0.036 4	0.055 1	0.004 6	321	5	333	31
12	4	67	0.563 3	0.051 0	0.000 6	0.406 5	0.034 2	0.057 8	0.004 8	321	4	346	29
13	5	204	1.145 6	0.020 2	0.000 2	0.138 0	0.010 1	0.049 6	0.003 6	129	1	131	10
14	3	52	0.706 9	0.051 3	0.000 8	0.398 8	0.032 9	0.056 4	0.004 5	322	5	341	28
15	3	43	0.596 5	0.050 6	0.000 7	0.392 1	0.031 8	0.056 3	0.004 8	318	4	336	27
16	10	263	0.950 3	0.025 8	0.000 3	0.423 8	0.010 2	0.119 3	0.002 5	164	2	359	9
17	30	194	0.846 7	0.143 4	0.001 4	1.336 3	0.026 0	0.067 6	0.001 3	864	8	862	17
18	14	269	0.316 9	0.051 5	0.000 4	0.377 2	0.010 0	0.053 1	0.001 4	324	3	325	9

Table 2 Analytical U-Pb zircon data of diorites (PM105-17TW2) from West Ujimqin

Spot	Content (ppm)		$^{232}Th/^{238}U$	Isotope ratios						Apprent ages (Ma)			
	Pb	U		$^{206}Pb/^{238}U$	1σ	$^{207}Pb/^{235}U$	1σ	$^{207}Pb/^{206}Pb$	1σ	$^{206}Pb/^{238}U$	1σ	$^{207}Pb/^{235}U$	1σ
1	3	67	0.125 9	0.051 5	0.005	0.377 3	0.027 3	0.053 2	0.003 9	323	3	325	24
2	14	285	0.239 3	0.051 3	0.007	0.374 2	0.014 0	0.053 0	0.001 9	322	4	323	12
4	14	272	0.436 3	0.050 7	0.005	0.368 6	0.007 7	0.052 7	0.001 1	319	3	319	7
5	18	342	0.443 6	0.051 1	0.005	0.368 3	0.009 1	0.052 3	0.001 2	321	3	318	8
6	7	140	0.261 2	0.050 8	0.005	0.372 1	0.014 5	0.053 1	0.002 1	320	3	321	12
7	37	738	0.400 3	0.050 5	0.005	0.369 9	0.003 8	0.053 1	0.000 5	318	3	320	3
8	79	1455	0.662 9	0.051 1	0.005	0.368 4	0.006 8	0.052 3	0.001 0	321	3	318	6
9	17	351	0.314 4	0.050 8	0.004	0.371 1	0.005 8	0.053 0	0.000 8	319	3	320	5
10	23	470	0.314 4	0.050 3	0.005	0.375 3	0.008 2	0.054 1	0.001 2	317	3	324	7
11	19	381	0.300 3	0.050 6	0.005	0.365 3	0.005 6	0.052 3	0.000 8	318	3	316	5
12	8	157	0.390 6	0.050 4	0.005	0.374 6	0.013 2	0.053 9	0.001 9	317	3	323	11
13	16	322	0.403 0	0.050 4	0.005	0.366 1	0.010 6	0.052 7	0.001 5	317	3	317	9
14	7	147	0.123 7	0.050 9	0.006	0.389 9	0.026 5	0.055 6	0.003 4	320	4	334	23
15	12	251	0.280 4	0.050 7	0.004	0.371 2	0.021 6	0.053 0	0.003 1	319	3	321	19
16	105	218	0.632 5	0.429 2	0.000	9.523 0	0.177 5	0.160 9	0.002 8	2302	22	2390	45
17	44	848	0.568 8	0.050 9	0.005	0.369 0	0.006 4	0.052 5	0.000 9	320	3	319	5
18	19	381	0.316 9	0.051 2	0.006	0.368 6	0.017 6	0.052 2	0.002 0	322	4	319	15

3.2 Major and Trace Element Compositions

The geochemical and analytical results of gabbro and diorite are shown in Table 3. The coordinates of the gabbro samples (PM103-2YQ1, PM103-3YQ1, PM103-3YQ2) are, in order, (44°16′02″N, 117°55′09″E), (44°15′59″N, 117°54′55″E), (44°15′33″N, 117°55′15″E). The diorite samples (PM105-4YQ1, PM105-9YQ1, PM105-16YQ1) are located successively at (44°15′17″N, 117°41′18″E), (44°15′12″N, 117°41′32″E) and (44°14′58″N, 117°42′23″E).

3.2.1 Major elements

The SiO_2 contents of gabbro samples span a range of 48.3% to 51%, and the gabbros were classified as mafic intrusive rocks. The TiO_2 contents range from 0.45% to 0.99%, with an average of 0.66%. The Al_2O_3 contents range from 14.48% to 16.98%, with an average of 15.62%. The gabbros have characteristic of high alumina basalt. These samples are rich in Na but poor in K ($Na_2O/K_2O>4.9$), with Na_2O=2.26%–3.73% and K_2O=0.11%–0.3%. The CaO contents span a range of 9.16% to 11.27%. The gabbros have relatively high MgO (8.06%–9.33%), with $Mg^{\#}$ values of 61.43 to 71.15, and SI values of 39.45 to 46.86. The $Mg^{\#}$ and SI values are close to mantle-derived magma. In the TAS diagram (Fig. 6), all of the samples with σ values of 1.11 to 1.92 fell into the sub-alkaline gabbro field. In the AFM diagram (Fig. 7), two samples were classified as tholeiite series and one was classified as

calc-alkaline series. However, all samples have high loss on ignition (LOI) (2.42%–3.71%) and Na_2O contents (2.26%–3.73%), indicating different degrees of alteration after diagenesis.

The SiO_2 contents of diorite samples span a range of 54.23% to 59.33 %, and the diorites were thus classified as intermediate intrusive rocks. The TiO_2 contents range from 0.68% to 0.92%, with an average of 0.82%. The Al_2O_3 contents range from 15.34% to 17.36%, with an average of 16.15%. These samples are rich in Na but poor in K (Na_2O/K_2O=4.6–13.3), with Na_2O=2.26%–3.73% and K_2O=0.23%–0.51%. The CaO contents span a range of 6.13% to 9.18%. The diorites have relatively low MgO (2.78%–3.86%), with $Mg^{\#}$ values of 35.76 to 45.63 and SI values of 19.13 to 21.97. In the TAS diagram (Fig. 6), all of the samples with σ values of 0.52 to 0.98 were plotted in the field of sub-alkaline gabbro diorite and diorite. In the AFM diagram (Fig. 7), two samples were classified as tholeiite series and one as calc-alkaline series. Similar to gabbros, all of the diorites underwent different degrees of alteration after diagenesis.

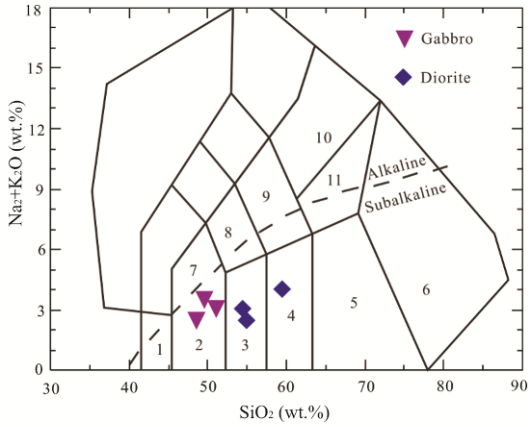

Figure 6. TAS diagram (Wilson, 1989). 1. olive gabbro; 2. sub-alkaline gabbro; 3. gabbro diorite; 4. diorite; 5. granodiorite; 6. granite; 7. alkaline gabbro; 8. monzodiorite; 9. secondary feldspar gabbro; 10. syenite; 11. quartzmonzonite.

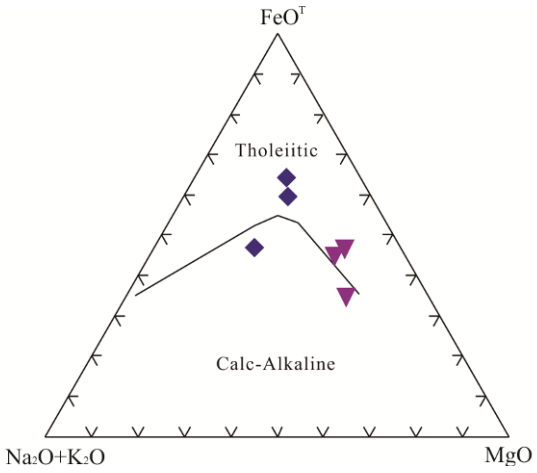

Figure 7. AFM diagram (Pearce, 1996).

3.2.2 Trace elements

In the mid-ocean ridge basalt (MORB)-normalized trace element spider diagrams (Fig. 8a), the gabbros and diorites show moderate enrichment in LILE (e.g., Rb, Ba, K and Sr) and negative Nb and Ta anomalies. These features resemble volcanic arc basalt and indicate that the magma source probably experienced metasomatism by the subduction fluid (Wilson M., 1989; Jacks and White, 1972). In the primitive mantle-normalized trace element spider plots (Fig. 8b), these samples are enriched in LILE and depleted in HFSE (e.g., Th, Nb, Ta, Ti and P), especially showing distinctly negative Nb and Ta anomalies. The spider diagrams are similar to arc magmatic trace element distribution patterns (Sun and McDonough, 1989).

3.2.3 Rare earth elements

The rare earth element contents of the gabbros range from 28.02 ppm to 45.66 ppm, and the $(La/Yb)_N$ ratios range from 0.48 to 0.68, with LREE/HREE=0.48–0.55. They display moderately to weakly positive Eu anomalies (δEu=1.32–1.57). The positive Eu anomalies are mainly caused by the accumulation of plagioclase in a magma chamber. The LREEs experienced moderate to weak fractional distillation ($(La/Sm)_N$=0.52–0.66), whereas the HREE slack fractional distillation ($(Gd/Yb)_N$= 0.84–0.94). The abundances of rare earth elements of the diorites range from 48.74 ppm to 83.52 ppm, which are relatively higher than those of the gabbros. Additionally, the $(La/Yb)_N$ ratios range from 0.6 to 1.43, with LREE/HREE=0.54–1.05. They display weakly negative Eu anomalies (δEu=0.95–1.26) indicating the accumulation of plagioclase. The LREEs underwent moderate to weak fractional distillation ($(La/Sm)_N$= 0.61–1.05), whereas the HREEs lack fractional distillation ($(Gd/Yb)_N$=0.85–1.06).

The chondrite-normalized REE distribution patterns (Fig. 9) show that all gabbro and diorite samples display uniform REE patterns, exhibiting relatively depleted LREE similar to N-MORB (Sun and McDonough, 1989; Pearce, 1982), which indicates that the magma derived from a depleted mantle source similar to N-MORB.

4 DISCUSSION

4.1 Effects of Alteration on Elemental Mobility

The gabbros and diorites aged ~321 Ma old must have been altered to various degrees after their emplacement, judging from petrographic observation and high contents of LOI (N2.4 wt.%, Table 3). High-field strength elements (e.g., Ti, Zr, Y, Th, Nb and REE) in rocks are relatively immobile under conditions of low-temperature alteration (Hofmann, 1997; Bienvenu et al., 1990; Condie, 1989; Winchester and Floyd, 1977; Pearce and Cann, 1973). The low-grade metamorphism is considered to have had an insignificant effect on REE and HFSE of the West Ujimqin gabbros and diorites. Furthermore, all the samples have uniform HFSE abundances, indicating that the gabbros and diorites still preserve their original HFSE signatures. Therefore, HFSEs are used in the following discussion to characterize the samples with respect to their original composition and possible tectonic setting (Frey et al., 2002; Meschede, 1986; Pearce and Cann, 1973).

Table 3 Major and trace element abundances of gabbros and diorites from West Ujimqin

Sample No.	PM103-2YQ1	PM103-3YQ1	PM103-3YQ2	PM105-4YQ1	PM105-9YQ1	PM105-16YQ1
	Gabbro	Gabbro	Gabbro	Diorite	Diorite	Diorite
Major elements (wt.%)						
SiO_2	49.38	51.00	48.34	54.87	54.23	59.33
Al_2O_3	16.98	14.48	15.41	15.34	15.76	17.36
TiO_2	0.54	0.45	0.99	0.92	0.87	0.68
Fe_2O_3	2.72	3.28	3.10	6.81	4.85	2.99
FeO	4.36	6.04	6.54	4.14	5.82	3.28
CaO	9.16	10.99	11.27	9.18	7.84	6.13
MgO	9.33	8.06	8.25	3.18	3.86	2.78
K_2O	0.3	0.17	0.11	0.23	0.51	0.28
Na_2O	3.2	2.88	2.32	2.26	2.53	3.73
MnO	0.13	0.15	0.17	0.21	0.18	0.12
P_2O_5	0.03	0.03	0.06	0.17	0.08	0.16
LOI	3.71	2.42	3.40	2.62	3.41	3.10
Total	99.86	99.94	99.93	99.92	99.93	99.94
A/CNK	0.76	0.58	0.63	0.74	0.83	0.99
σ	1.92	1.16	1.11	0.52	0.82	0.98
$Mg^{\#}$	71.15	61.75	61.43	35.76	40.57	45.63
SI	46.86	39.45	40.6	19.13	21.97	21.29
Trace elements (ppm)						
V	149.5	177.2	255.2	207.8	299	112.9
Cr	500	151.5	113.6	21.9	9.8	16.5
Co	31.5	38.3	38.1	26.4	29.1	15.4
Ni	84.3	53.9	49.9	11.6	8.8	9.2
Cu	23.3	13.0	55.5	63.7	58.9	27.8
Zn	39.0	49.9	55.2	106.6	92.9	74.3
Ga	10.12	12.04	14.41	17.99	17.87	17.5
Rb	5.0	2.8	1.8	4.3	11.0	5.3
Sr	98.7	112.4	91.4	379.1	150	308.8
Zr	38.8	32.6	56	67.9	56.3	87.9
Nb	0.34	0.33	0.61	2.07	1.48	1.02
Cs	0.43	0.27	0.35	0.61	0.34	1.41
Ba	81.7	46.3	36.6	80.6	128.8	58.4
Hf	1.49	1.17	1.94	3.54	3.67	5.86
Ta	0.05	0.04	0.06	0.15	0.14	0.08
Pb	0.9	0.9	1.0	4.1	3.3	2.6
Th	0.13	0.11	0.11	0.74	0.5	0.58
U	0.04	0.05	0.07	0.35	0.26	0.12
Rare earth elements (ppm)						
La	1.08	0.97	2.00	6.11	2.91	3.01
Ce	3.04	2.88	5.00	13.87	8.14	8.08
Pr	0.53	0.51	0.96	2.33	1.49	1.39

Table 3 Continued

Sample No.	PM103-2YQ1	PM103-3YQ1	PM103-3YQ2	PM105-4YQ1	PM105-9YQ1	PM105-16YQ1
	Gabbro	Gabbro	Gabbro	Diorite	Diorite	Diorite
Nd	3.15	3.08	5.45	12.56	8.58	7.53
Sm	1.17	1.18	1.91	3.66	2.98	2.3
Eu	0.6	0.66	0.9	1.27	0.99	0.93
Gd	1.41	1.43	2.23	3.8	3.44	2.22
Tb	0.33	0.34	0.52	0.81	0.79	0.48
Dy	2.28	2.28	3.55	5.11	5.24	3.02
Ho	0.5	0.53	0.79	1.17	1.24	0.68
Er	1.35	1.43	2.18	3.03	3.39	1.82
Tm	0.25	0.27	0.41	0.61	0.67	0.36
Yb	1.21	1.36	1.98	2.88	3.28	1.79
Lu	0.18	0.20	0.30	0.40	0.48	0.26
Y	10.96	11.50	17.47	25.93	27.95	14.88
∑REE	28.02	28.63	45.66	83.52	71.59	48.74
LREE/HREE	0.52	0.48	0.55	0.91	0.54	0.91
$(La/Yb)_N$	0.60	0.48	0.68	1.43	0.6	1.13
δEu	1.43	1.57	1.32	1.04	0.95	1.26
La_N/Sm_N	0.58	0.52	0.66	1.05	0.61	0.82
Gd_N/Yb_N	0.94	0.84	0.91	1.06	0.85	1.00
Rb_N/Yb_N	4.15	2.05	0.91	1.49	3.35	2.95
Zr/Nb	114.12	98.79	91.8	32.8	38.04	86.18
La/Nb	3.16	2.94	3.28	2.95	1.96	2.95
La/Ta	21.50	24.23	33.38	40.70	20.77	37.68

A/CNK=$(Al_2O_3/102)/((CaO/56)+(K_2O/94)+(Na_2O/62))$; $Mg^{\#}=(MgO/40)/((MgO/40+FeO/72+Fe_2O_3\times0.899$ 8/160)×100; SI=100×MgO/(MgO+FeO+Fe_2O_3+K_2O+Na_2O); $\sigma=(K_2O+Na_2O)\times(K_2O+Na_2O)/(SiO_2-43)$; the subscript N represents chondrite-normalized, after Boynton (1984).

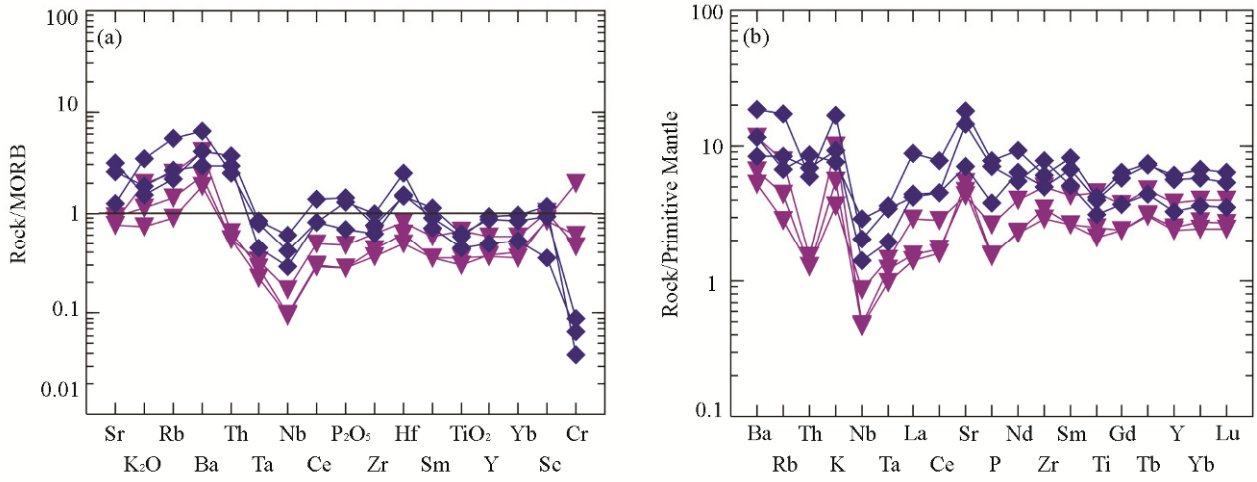

Figure 8. (a) MORB-normalized trace element spider diagram (Pearce, 1982); (b) primitive mantle-normalized trace elements spider diagram (Sun and McDonough, 1989).

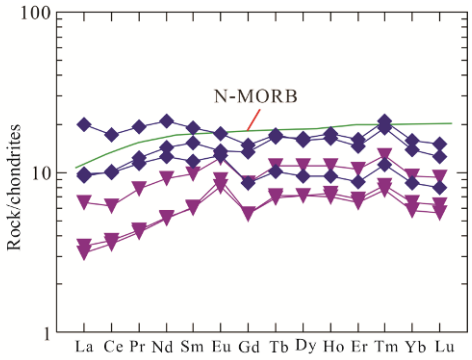

Figure 9. Chondrite-normalized REE pattern (Boynton, 1984) and the N-MORB parameter after Sun and McDonough (1989).

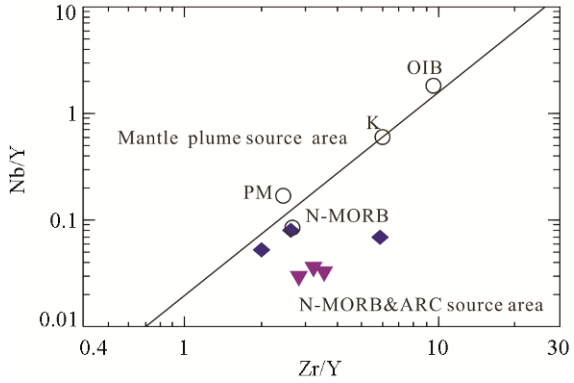

Figure 10. Nb/Y-Zr/Y diagram (Zhu et al., 2008); the boundary of the mantle plume, N-MORB and ARC source regions are after Fitton et al. (1997); the parameters of OIB, N-MORB and PM are derived from Sun and McDonough (1989); K represents the Kerguelen mantle plume.

4.2 Petrogenesis

The gabbro and diorite plutons from West Ujimqin have low REE contents and display a slight LREE depletion on the chondrite-normalized REE diagrams. All of these features are similar to normal mid-ocean ridge basalt (N-MORB) (Sun and McDonough, 1989; Pearce, 1982). The Zr/Nb ratio of N-MORB is always greater than 30, and the ratios of the samples of this study are all greater than 30 (32.8–114.12, average of 77), suggesting that the magma was derived from a depleted mantle source area. Fitton et al. (1997) have successfully developed the robust ΔNb approach (excess or deficiency in Nb, ΔNb=1.74+log (Nb/Y)−1.92log (Zr/Y)) to identify the mantle source of mafic rocks. Mafic magmas derived from plume exhibit ΔNb>0, whereas magmas derived from depleted mantle show ΔNb<0 (Baksi, 2001; Fitton et al., 1997). The ΔNb values for the gabbros and diorites of this researched area are less than 0, suggesting that the magma is probably derived from a depleted mantle. Furthermore, in the Nb/Y-Zr/Y diagram (Fig. 10), the samples are plotted in the N-MORB and ARC fields. In general, the average La/Nb and La/Ta ratios of the asthenospheric (lithospheric) mantle are less (greater) than 1.5 and 22, respectively (Huang et al，2000). The La/Nb (1.96–3.28) and La/Ta (20.77–44.64) ratios of West Ujimqin gabbros and diorites suggest that the magma was derived from the asthenospheric mantle. Generally, crustal rocks have low TiO_2 contents (average of 0.72%) (Rudnick and Gao, 2003); the TiO_2 content of the asthenosphere is approximately 1.27% (Sun and McDonough, 1989), and the TiO_2 content of the deep mantle is always greater than 2% (Zhu et al., 2008). The low TiO_2 content (0.45%–0.99%, averaging 0.74%) of West Ujimqin gabbros and diorites indicate that the magmatic source is mainly related to the shallow depleted mantle.

Generally, with the increasing of partial melting of the spinel lherzolite, the residual mantle blocks and melts have similar Sm/Yb ratios, whereas the La/Sm ratio decreases (Aldanmaz et al., 2000). Therefore, the partial melting of the spinel lherzolite results in a relatively horizontal melting trend (i.e., near the mantle). However, the Sm/Yb ratio will increase sharply if a mid-low degree of partial melting of the garnet lherzolite happens, the Sm/Yb ratio of the melt increases rapidly. Thus, the melting trend of the garnet lherzolite obviously deviates from that of the mantle (Zhu et al., 2008; Aldanmaz et al., 2000). On the Sm/Yb vs. La/Sm diagram (Fig. 11a), the points lie parallel to the partial melting curve of the spinel lherzolite, which demonstrates that the magmas of the gabbros and diorites from West Ujimqin mainly derived from moderate (5%–20%) partial melting of the spinel lherzolite.

On MORB-normalized and primitive mantle-normalized trace elements spider diagrams (Figs. 8 and 9), the gabbros and diorites both exhibit characteristics of enriched in LILE (e.g., Rb, Ba, K, Sr) but depleted in Nb, Ta and Ti. These features are similar to those of arc-related magma genesis (Kelemen et al., 2003). Therefore, the shallow depleted mantle derived magma probably contaminated by subduction-related materials and underwent metasomatism. On the La/Nb vs. La/Ba diagram (Fig. 11b); the results may indicate the signatures of a subduction-modified mantle source. As shown in Fig. 12a, the samples are plotted in the field of sediments and subduction zone magmas, indicating the source may have endured the influence of sediments before partial melting (Rottura et al., 1998). This conclusion is further supported by the result on Ta/La vs. Ce/Pb and Ba/Rb vs. Nb/La diagrams (Figs. 12b and 12c). The source was mainly affected by fluid metasomatism and contaminated by sediments (Oyhantcabal et al., 2007). Furthermore, on the Nb/Y vs. La/Nb diagram (Fig. 12d), all samples plots into the fluid-induced metasomatism field, showing that the depleted mantle source was mainly metasomatized by subducted slab-released fluids (Hoffer et al., 2008).

4.3 Tectonic Significance

Zircon LA-ICP-MSU-Pb ages of the gabbro and diorite from West Ujimqin indicate the plutons emplaced at 321±2.0 and 319.4±1.5 Ma, respectively. The zircons were all crystallized, and no inherited cores were observed in the CL images. Therefore, the zircon U-Pb ages can represent the formation time of the rocks. Quartz diorite pluton is unconformably covered by Upper Carboniferous Benbatu and Amushan Formations and it intrudes into the diorite pluton. This also verifies the accuracy of the isotopic ages. The gabbros and diorites have similar geochemical characteristics. All of the features aforementioned indicate that the gabbros and diorites should be of synchronous magmatism occurred during the late Early Carboniferous.

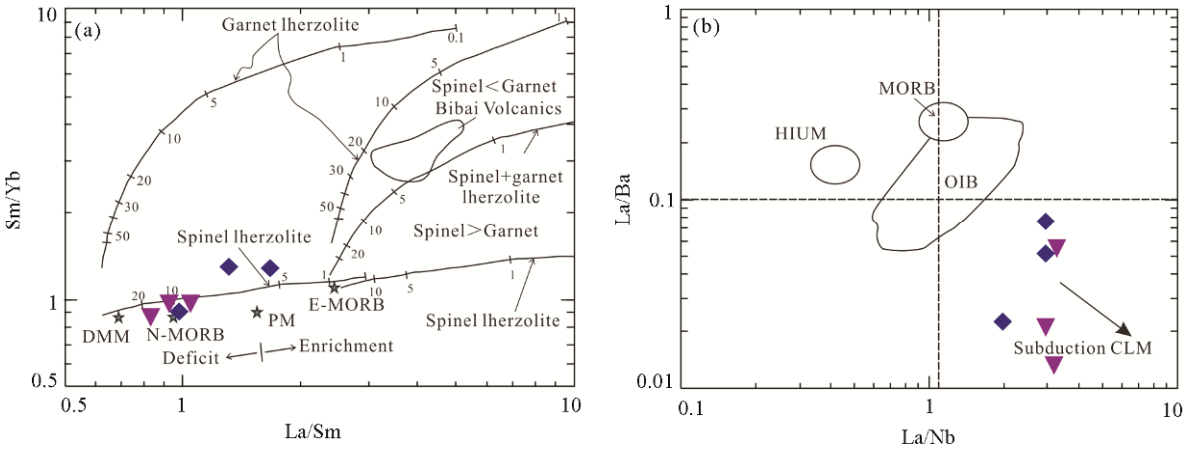

Figure 11. (a) Sm/Yb-La/Sm diagram after Zhu et al. (2008) and Aldanmaz et al. (2000); the parameters of PM, N-MORB and E-MORB are derived from Sun and McDonough (1989); (b) La/Ba-La/Nb diagram after Saunders (1992).

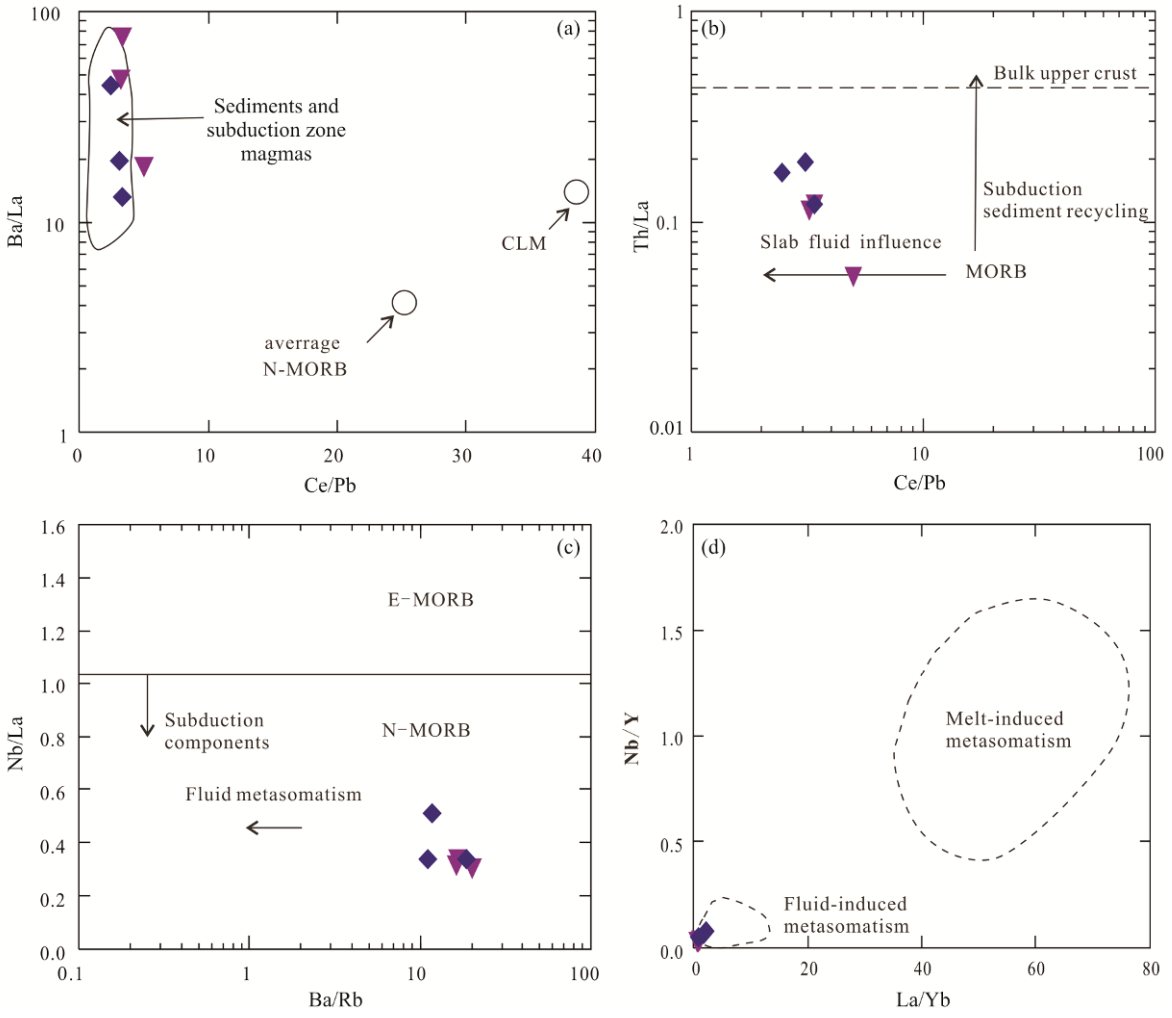

Figure 12. (a) Ce/Pb-Ba/La diagram (Rottera et al. 1998); (b) Ce/Pb-Th/La diagram (Oyhantcabal et al. 2000); (c) Ba/Rb-Nb/La diagram (Oyhantcabal et al. 2007); (d) La/Yb-Nb/Y diagram (Hoffer et al. 2008).

The gabbros and diorites are plotted on a series of discriminant diagrams using incompatible immobile trace elements to interpret the tectonic setting in which they formed.

On Nb×2-Zr/4-Y (Meschede, 1986) and Ti/100-Zr-Y×3 (Pearce and Cann, 1973) diagrams (Figs. 13a and 13b), the gabbros and diorites are plotted in the field of volcanic arc basalt and N-MORB. Nb, Yb, Ti and Zr discrimination diagrams have also been used by previous workers to discriminate MORB (N-MORB, E-MORB), OIB and non-arc mantle array (Parlak, 2016; Dai et al., 2011; Pollock and Hibbard, 2010;

Pearce, 2008; Pearce and Peate, 1995). The gabbro and diorite samples from West Ujimqin mainly fall within the field of N-MORB on TiO_2/Yb vs. Nb/Yb (Pearce, 2008) and Zr/Yb vs. Nb/Yb (Pearce and Peate, 1995) diagrams (Figs. 13c and 13d). The Hf/3-Th-Nb/16 plot (Wood, 1980) is used to distinguish island arc basalts (IAB), N-MORB, E-MORB and within plate alkaline basalts. Most samples are plotted (Fig. 13e) in the IAB field but near the field of N-MORB. Also they are displaced towards the Hf apex. The discrimination of magmas in this diagram results from the depleted mantle sources and high degrees of partial melting. In addition, on the Th/Yb-Nb/Yb (Pearce and Peate, 1995) diagram (Fig. 13f), all samples plot in the field of volcanic arc basalt but near the field of N-MORB.

The results from tectonic setting discrimination diagrams discussed above reveal that the gabbros and diorites display both characteristics of volcanic arc basalt and MORB, which consistent with their geochemical characteristics. These attributes all indicate that a component from a depleted MORB-like mantle was involved in their generation. In view of the above, a depleted mantle-related magmatism associated to an expanding oceanic system should have been active where West Ujimqin gabbros sand diorites originated. However, very small volumes of such rocks are poorly recognized up to now suggesting that plume activity might have been limited.

Basaltic rocks with both characteristics of arc-related basalt and MORB can be generated under three kinds of tectonic settings as follows: (1) extensional mid-oceanic ridge related to the ridge subduction, e.g. tholeiitic basalt generated by the subduction of South Chile mid-oceanic ridge (Karsten, 1996); (2) extensional back-arc basin (Ma et al., 2015; Yan et al., 2015; Jeffrey et al., 2010); (3) immature juvenile oceanic basin (Chen et al., 2012). Previous researches have revealed that the Paleo-Asian Oceanic basin have closed before the Carboniferous, and then epicontinental sea and rifts developed in XMOB rather than mid-oceanic ridge and back-arc basin (Xu et al., 2014; Shao et al., 2014, 1991; Bao et al., 2006; Su, 1996; Cao et al., 1986). The gabbros and diorites in the study area show geochemical characteristics of basaltic rocks from an immature newly-born oceanic basin.

Intense rifting magmatic activities occurred in XMOB during the Carboniferous-Permian (Shao et al., 2014; Xu et al., 2014; Tang, 1989). Published data show that there were widespread mafic rocks, alkali granites, and bimodal volcanic rocks under the rift setting during this period (Cheng et al., 2014; Feng et al., 2014; Chen et al., 2012; Tang et al., 2011; Jahn et al., 2009; Yarmolyuk et al., 2008). All of these features are in accordance with the post-orogenic magmatism (Zhang et al., 1999; Liegeois, 1998). Additionally, West Ujimqin Baiyingaole Carboniferous quartz diorite with age of 323 Ma was generated under an extensional tectonic setting after the collision between the North China and Siberian plates (Bao et al., 2007). In this study, the gabbros and diorites with ages of 321 and 319.4 Ma, respectively, are in accordance with the scope of the above age for Carboniferous quartz diorite (Bao et al., 2007). Furthermore, the Carboniferous–Permian strata in West Ujimqin are contemporaneous, but the heteropic strata in the sea trough formed under an intracontinental depression (possibly rift) setting (Li et al., 2015; Bao et al., 2006).

The newly discovered ultrabasic and mafic rocks are similar to the newly identified West Ujimqin Diyanmiao ophiolite (Li et al., 2013, 2012b,) in terms of geochemical characteristics (Dong, 2014). They probably represent the remnant ocean crust of this region. Bai (2013) reported a zircon LA-ICP-MS U-Pb age of 320 Ma for the gabbro from Diyanmiao ophiolite in West Ujimqin, in accordance with the zircon ages of the gabbros in this study, and with similar similar geochemical signatures. This suggests that they originated from the same magma chamber and formed under the same tectonic setting. Accordingly, the gabbros of this study may be a part of the ophiolite complex, so the age obtained in this study should represent the formation age of ophiolite in this area. Under an intense extensional rift (Su, 1996), and a new ocean basin may have opened due to the thin continental crust or a deeper rift after further extension. The ophiolite complex in the study area probably developed in a deeper part of the rift, which further developed to an immature newly-born oceanic basin. The gabbros and diorites from West Ujimqin show geochemical characteristics both of N-MORB and subduction-related arc magmatic rocks with contamination and metasomatism. On the basis of comprehensive contrast analysis and combined with previous researches, we deemed that the Early Carboniferous magmatism in West Ujimqin occurred under a new immature ocean basin.

The mafic rocks from Mandula and Hegenshan formed in an extensional rift setting in the Early Permian, and the Solonker-Hegenshan belt probably had already developed into a new Red Sea-like oceanic basin after further development (Chen et al., 2012). The geochemical characteristics of the mafic rocks in this study are comparable to those of Mandula and Hegenshan mafic rocks, which indicate that a new incipient ocean basin opened in some parts of the Mandula-Hegenshan region under an intense extensional rift setting in the late Early Carboniferous.

5 CONCLUSIONS

The LA-ICP-MS zircon U-Pb age of the gabbros and diorites from West Ujimqin are 321±2.0 and 319.4±1.5 Ma, respectively, belonging to the late Early Carboniferous.

The gabbros and diorites from West Ujimqin show slightly LREE-depleted chondrite-normalized REE patterns similar to N-MORB, with low TiO_2 contents (average of 0.71%), La/Nb>1.5，La/Ta>22, indicating that the magma was derived from the shallow depleted lithospheric mantle. However, these samples are LILE (e.g., Rb, Ba and Sr) enriched and HFSE depleted, suggesting that the magmatic source probably underwent subduction-related contamination and metasomatism. The magma generated from moderate (5%–20%) partial melting of the spinel lherzolite.

On the basis of geochemical characteristics of the samples in this study, combined with regional geological data and previous researches, we believe that the Early Carboniferous gabbros and diorites from West Ujimqin formed under an intense extensional rift setting in the late Early Carboniferous, and a new limited incipient oceanic basin opened in West Ujimqin.

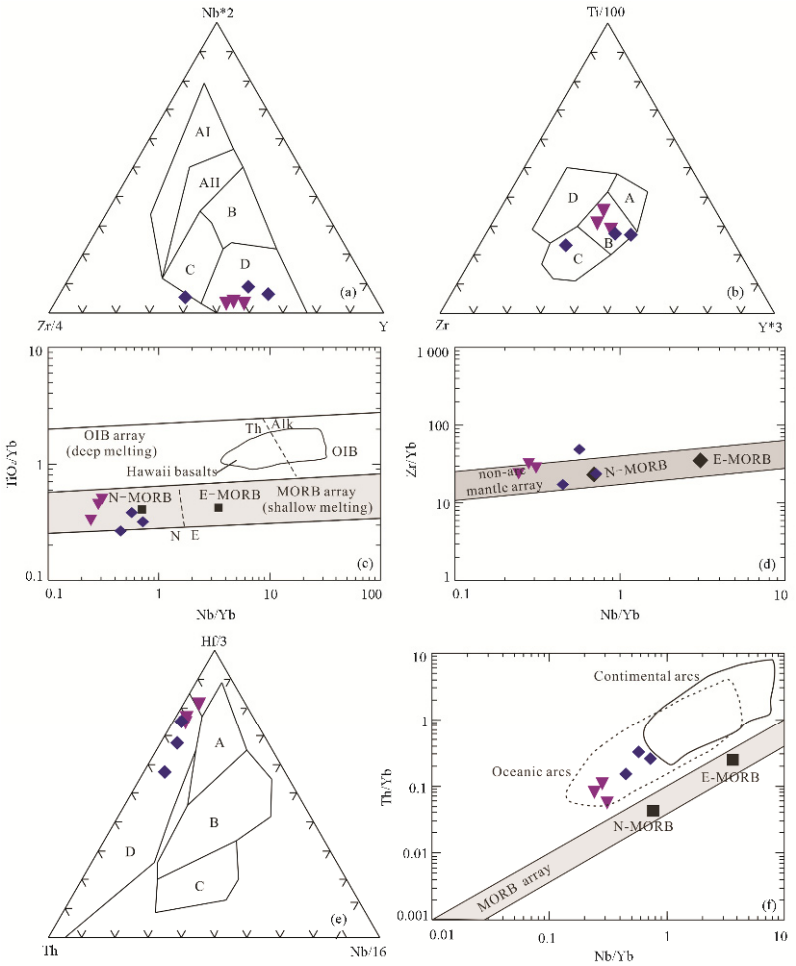

Figure 13. Tectonic discrimination diagrams (a) Nb×2-Zr/4-Y variation diagram (Meschede, 1986). AI. within-plate alkali basalts; AII. within-plate alkali basalts and within-plate tholeiites; B. E-type MORB; C. within-plate tholeiites and volcanic-arcbasalts; D. N-MORB and volcanic-arc basalts. (b) Ti/100-Zr-Y×3 discrimination diagram (Pearce and Cann, 1973). A. island-arc tholeiites; B. MORB+island-arctholeiites+island-arc calc-alkali basalts; C. island-arc calc-alkali basalts; D. within-plate basalts. (c) TiO_2/Yb-Nb/Yb diagram (Pearce, 2008). (d) Trace element plot of Zr/Yb vs Nb/Yb (Pearce and Peate, 1995). (e) Hf/3-Nb/16-Th plot (Wood, 1980). A. N-MORB; B. E-MORB; C. within plate alkaline basalts; D. island-arc tholeiites. (f) Th/Yb vs Nb/Yb diagram (Pearce and Peate, 1995)

ACKNOWLEDGMENTS

We thank the editors and reviewers. We wish to express our gratitude to senior engineer Neng Zhang, Prof. Dezhen Gao and engineer Ruijie Li for their help with the manuscript and field work. Thanks to Dr. Xuxuan Ma, Zhiyu Yi, Chen Wu, Huawen Cao and Zhihui Liu, assistant engineer Yang Du and Baoxia Li for their important help during the study. This research was supported by the National Science Foundation of China (No. 49021001), the Public Welfare Profession Foundation of Ministry of Land and Resources (Nos. 201511022, 201211093) and the Geological Survey of China (Nos. 12120115026801, 1212011120700, 1212011220465, 12120114093901). The final publication is available at Springer via http://dx.doi.org/10.1007/s12583-016-0912-2.

REFERENCES CITED

Aldanmaz, E., Pearce, J. A., Thirlwall, M. F., et al., 2000. Petrogenetic Evolution of Late Cenozonic, Post-Collision Volcanism in Western Anatolia, Turkey. *Journal of Volcanology and Geothermal Research*, 102(1–2): 67–95. doi:10.1016/s0377-0273(00)00182-7

Badarch, G., Dickson, C. W., Windley, B. F., 2002. A New Terrane Subdivision for Mongolia: Implications for the Phanerozoic Crustal Growth of Central Asia. *Journal of Asian Earth Sciences*, 21(1): 87–110. doi:10.1016/s1367-9120(02)00017-2

Bai, H., 2013. The Petrological and Geochemical Characteristics of Ophiolite on the Area of Diyanmiao in the Inner Mongolia: [Dissertation]. Shijiazhuang University of Economics, Shijiazhuang. 1–59 (in Chinese with English Abstract)

Baksi, A. K., 2001. Searth for a Deep-mantle Component in Mafic Lavas Using an Nb-Y-Zr Plot. *Canadian Journal of Earth Sciences*, 38(5):813–824. doi:10.1139/cjes-38-5-813

Bao, Q. Z., Zhang, C. J., Wu, Z. L., et al., 2006. Carboniferous-Permian Marine Lithostratigraphy and Sequence Stratigraphy in Xi Ujimqin Qi, Southeastern Inner Mongolia, China. *Geological Bulletin of China*, 25(5):572–579 (in Chinese with English Abstract)

Bao, Q. Z., Zhang, C. J., WU, Z. L., et al., 2007. SHRIMP U-Pb Zircon Geochronology of a Carboniferous Quartz-Diorite in Baiyingaole Area，Inner Mongolia and Its Implications. *Journal of Jilin University* (*Earth Science Edition*), 37(1): 15–23 (in Chinese with English Abstract).

Bienvenu, P., Bougault, H., Joron, J., et al., 1990. MORB Alteration: Rare-Earth

Element/Non-Rare-Earth Hygromagmaphile Element fractionation. *Chemical Geology* 82(1–2): 1–14. doi:10.1016/0009-2541(90)90070-n

Cabanis, B., Lecolle, M., 1989. Le Diagramme La/10-Y/15-Nb/8: Unoutil pour la Discrimination de Series Volcaniqueset la Miseenmiseen Evidence Desprocessus de Mélange et/ou de Contamination Crustale. The La/10–Y/15–Nb/8 Diagram: A Tool for Distinguishing Volcanic Series and Discovering Crustal Mixing and/ or Contamination. Comptes Rendus de I'Academie des Sciences, Series 2, Mecanique , Physique, Chimie, Sciences de l'Univers, *Sciences de la Terre*, 309(20): 2023–2029

Cai, K. D., Yuan, C., Sun, M., et al., 2007. Geochemical Characteristics and ^{40}Ar-^{39}Ar Ages of the Amphibolites and Gabbros in Tarlang Area: Implications for Tectonic Evolution of the Chinese Altai. *Acta Petrological Sinica*, 23 (5): 877–888 (in Chinese with English Abstract)

Cao, C. Z., 1986. The Ophiolite in Hegenshan district, Nei Mongol and the Position of Suture Line between Sino-Korean and Siberian Plates. In: Cao, C. Z., Yang, F. L., Tian, C. L., eds., Proceedings of North China Plate Tectonics, 1 set. *Beijing: Geological Publishing House*, 64–86 (in Chinese with English Abstract)

Chen, B., Jahn B. M., Wilde, S. A., et al., 2000. Two Contrasting Paleozonic Magmatic Belts in Northern Inner Mongolia, China: Petrogenesis and Tectonic Implications. *Tectonophysics*, 328(1–2): 157–182. doi:10.1016/s0040-1951(00)00182-7

Chen, B., Zhao, G. C., Simon WILDE. 2001. Subduction- and Collision-Related Granitoids from Southern Sonidzuoqi, Inner Mongolia: Isotopic Ages and Tectonic Implications. Geological Review, 47(4): 361–367 (in Chinese with English Abstract)

Chen, C., Zhang, Z. C., Guo, Z. J., et al., 2012.Geochronology, Geochemistry, and Its Geological Significance of the Permian Mandula Mafic Rocks in Damaoqi, Inner Mongolia. *Sci China Earth Sci*, 55(1): 39–52 (in Chinese with English Abstract)

Cheng, Y. H., Teng, X. J., Li, Y. F., et al., 2014. Early Permian East-Ujimqin Mafic-Ultrafic and Granitic Rocks from the Xing'an-Mongolian Orogenic Belt, North China: Origin, Chronology, and Tectonic Implications. *Journal of Asian Earth Sciences*, 96: 361–373. doi:10.1016/j.jseaes.2014.09.027

Condie K. C., 1989. Geochemical Changes in Basalts and Andessites across the Archaean-Proterozoic Boundary: Identification and Significance. *Lithos*, 23(1): 1–18. doi:10.1016/0024-4937(89)90020-0

Dai, J. G., Wang C. S., Hebert, R., et al., 2011. Late Devonian OIB Alkaline Gabbro in the Yarlung Zangbo Suture Zone: Remnants of the Paleo-Tethys? *Gondwana Research*, 19(S1): 232–243. doi:10.1016/j.gr.2010.05.015

Dong, J. Y., 2014. Characteristics and Geological Significance of Ophiolite on the Area Daqingmuchang in Xiwuqi, Inner Mongolia: [Dissertation]. China University of Geosciences, Beijing. 1–56 (in Chinese with English Abstract)

Feng, Z. Q., Liu, Y. J., Han, G. Q., et al., 2014. The Petrogenesis of ~330 Ma Meta-Gabbro-Granite from the Tayuan Area in the Northern Segment of the Da Xing' an Mts and Its Tectonic Implication. *Acta Petrologica Sinica*, 30(7): 1982–1994 (in Chinese with English Abstract)

Fitton, J. G., Saunders, A. D., Norry, M. J., et al., 1997. Thermal and Chemical Structure of the Iceland Plume. *Earth and Planetary Science Letters*, 153(3–4):197–208. doi:10.1016/s0012-821x(97)00170-2

Frey, F. A., Weis, D., Borisova, A. Y. U., et al., 2002. Involvement of Continental Crust in the Formation of the Cretaceous Kerguelen Plateau: New Perspectives from ODP Leg120 sites. *Journal of Petrology*, 43(7): 1207–1239. doi:10.1093/petrology/43.7.1207

Hancher, J. M., Miller, C. F., 1993. Zircon Zonation Patterns as Revealed by Cathodoluminescence and Back Scattered Electron Images: Implications for Interpretation of Complex Crustal Histories. *Chemical Geology*, 110(1): 1–13. doi:10.1016/0009-2541(93)90244-d

Hoffer, G., Eissen, J. P., Beate, B., et al., 2008. Geochemical and Petrological Constrains on Rear-Arc Magma Genesis Processes in Ecuatdor: The Puyo Cones and Mera Lavas Volcanic Formation. *Journal of Volcanology and Geothermal Research*, 176(1): 107–118. doi:10.1016/j.jvolgeores.2008.05.023

Hofmann, A. W., 1997. Mantle Geochemistry: The Massage from Oceanic Volcanism. *Nature*, 385(6613): 219–229. doi:10.1038/385219a0

Hong, D. W., Wang, S. G., Xie, X. L., et al., 2003. Correlation between Continental Growth and the Supercontinental Cycle: Evidence from the Grains with Positive ε_{Nd} in the Central Asian Orogenic Belt. *Acta Geologica Sinica*, 77(2): 203–209 (in Chinese with English Abstract)

Huang, Y. M., Hawkesworth, C., Smith, I., et al., 2000. Geochemistry of Late Cenozoic Basaltic Volcanism in North land and Coromandel New Zealand Implications Formantle Enrichment Processes. *Chemioal Geology*, 164(3/4): 219–238. doi:10.1016/s0009-2541(99)00145-x

Jahn, B. M., Griffin, W. L., Windley, B. F., 2000a. Continental Growth in the Phanerozoic: Evidence from Central Asia. *Tectonophysics*, 328(328): 227. doi:10.1016/s0040-1951(00)00174-8

Jahn, B. M., Wu, F.Y., Chen, B., 2000b. Granitoids of the Central Asian Orogenic Belt and Continental Growth in the Phanerozoic. Trans. Roy. Soc. *Edinburgh. Earth Sci*, 91: 181–193. doi:10.1017/s0263593300007367

Jahn, B.M., Wu, F.Y., Chen, B., 2000c. Massive Granitoid Generation in Central Asia: Nd Isotope Evidence and Implication for Continental Growth in the Phanerozoic. *Episodes*, 23(2): 82–92

Jahn, B.M., Wu, F.Y., Chen, B., 2001. Growth of Asia in the Phanerozoic Nd Isotopic Evidence. *Gondwana Res*, 4(4): 640–642. doi:10.1016/s1342-937x(05)70442-1

Jahn, B. M., Windley, B., Natal'in, B., et al., 2004. Phanerozoic Continental Growth in Central Asia. *Journal* of *Asian Earth Sciences*, 23(5): 599–603. doi:10.1016/s1367-9120(03)00124-x

Jahn, B. M., Litvinovsky, B. A., Reichow, M., et al., 2009. Peralkaline Granitoid Magmatism in the Mongolian-Transbaikanlian Belt: Evolution, Petrogenesis and Tectonic Significance. *Lithos*, 113(3–4): 521–539. doi:10.1016/j.lithos.2009.06.015

Jakes, P., White, A. J. R., 1972. Major and Trace Element Abundance in Volcanic Rocks of Orogenic Areas. *Bull .Geol. Soc. Am*, 83(1972): 29–40. doi:10.1130/0016-7606(1972)83[29:mateai]2.0.co;2

Jian, P., Kröner, A., Windley, B. F., et al., 2010. Zircon Ages of the Bayankhongor Ophiolite Mélangeand Associated Rocks: Time Constraints on Neoproterozoic to Cambrian Accretionary and Collisional Orogenesis in Central Mongolia. *Precambr. Res.*, 177(1): 162–180. doi:10.1016/j.precamres.2009.11.009

Jian, P., Kröner, A., Windley, B. F., et al., 2012. Carboniferous and Cretaceous Mafic-Ultramafic Massifs in Inner Mongolia (China): A SHRIMP Zircon and Geochemical Study of the Previously Presumed Integral "Hegenshan Ophiolite". *Lithos*, 142–143: 48–66. doi:10.1016/j.lithos.2012.03.007

Jian, P., Liu, D. Y., Kröner, A., et al., 2008. Time Scale of an Early to Mid-Paleozoic Orogenic Cycle of the Long-Lived Central Asian Orogenic Belt, Inner Mongolia of China: Implications for Continental Growth. *Lithos*, 101(3): 233–259. doi:10.1016/j.lithos.2007.07.005

Karsten, J. K., Klein, E. M., Sherman, S. B., 1996. Subdution Zone Geochemical Characteristics in Ridge Basalts from the Southern Chile Ridge: Implication of Modern Ridge Subduction System for Archean. *Lithos*, 37(2): 143–161. doi:10.1016/0024-4937(95)00034-8

Koschek, G., 1993. Origin and Significance of the SEM Cathodoluminescence from Zircon. *Journal of Microscopy*, 171(3): 223–232. doi:10.1111/j.1365-2818.1993.tb03379.x

Li, H. K., Zhu, S. X., Xiang, Z. Q., 2010. Zircon U-Pb Dating on Tuff Bed from Gaoyuzhuang Formation in Yangqing, Beijing: Further constrains on the New Subdivion of the Mesoproterozoic Stratigraphy in the Northern North Chian Craton. *Acta Petrologica Sinica*, 26 (7): 2131–2140 (in Chinese with English Abstract).

Li, H. Y., Zhou, Z. G., Li, P. J., et al. 2015. A Late Carboniferous-Early Permian Extensional Event in Xi Ujimqin Qi, Inner Mongolia-Evidence from Volcanic Rocks of Dashizhai Formation. *Geotectonica Et Metallogenia*, 40(5): 996–1013

Li, P. C., Liu, Z. H., Li, S. C., et al., 2016. Geochronology, Geochemistry, Zircon Hf Isotopic Characteristics and Tectonic Setting of Hudugeshaorong Pluton in Balinyouqi, Inner Mongolia. *Earth Science—Journal of China University of Geosciences*, 41(12): 1995–2007 (in Chinese with English Abstract)

Li, J. Y., 2006. Permian Geodynamic Setting of Northeast China and Adjacent Regions: Closure of the Paleo-Asian Ocean and Subduction of the Paleo-Pacific Plate. *Journal of Asian Earth Sciences*, 26(3–4): 207–224. doi:10.1016/j.jseaes.2005.09.001

Li, Y. J., Wang, J. F., Li, H. Y., et al., 2012b. Recognition of Diyanmiao Ophiolite in Xi Ujimqin Banner, Inner Mongolia. *Acta Petrologica Sinica*, 28(4): 1281–1290 (in Chinese with English Abstract)

Li, Y. J., Wang, J. F., Li, H. Y., et al., 2013. Geochemical Characteristics of Baiyinbulage Ophiolite in Xi Ujimqin Banner, Inner Mongolia. *Acta Petrologica Sinica*, 29(8): 2719–2730 (in Chinese with English Abstract)

Li, S. Z., Santosh, M., Jahn, B. M., 2012a. Evolution of the Asian Continent and Its Continental Margins. *Journal* of *Asian Earth Sciences*, 47(1): 1–4. doi:10.1016/j.jseaes.2012.02.001

Liegeois, L. P., 1998. Preface-Some Words on the Post-Collisional Magmatism. *Lithos*, 45: 1500–1511

Liu, C. F, Wu, C., Zhu, Y., et al., 2015. Late Paleozoic–Early Mesozoic Magmatichistory of Central Inner Mongolia, China: Implications for the Tectonic Evolution of the Xingmeng Orogenic Belt, the Southeastern Segment of the Central Asian Orogenic Belt. J*ournal of Asian Earth Sciences*, http://dx.doi.org/10.1016/j.jseaes.2015.09.011.

Liu, C. F., Liu, W. C., Zhou, Z. G., et al., 2014. Geochronology, Geochemistry and Tectonicsetting of the Paleozoic–Early Mesozoic Intrusive in Siziwangqi, Inner Mongolia. *Acta Geologica Sinica*, 88(6): 992–1002 (in Chinese with English Abstract).

Liu, J. F., Chi, X. G., Zhang, X. Z., et al., 2009. Geochemical Characteristics of Carboniferous Quartz-Diorite in the Southern Xiwuqi Area, Inner Mongolia and Its Tectonic Significance. *Acta Geologica Sinica*, 83 (3): 365–376 (in Chinese with English Abstract)

Liu, J. L., Sun, F. Y., Wang, Y. D., et al., 2016. Tectonic Setting of Hadahushu Mafic Intrusion in Urad Zhongqi Area, Inner Mongolia: Implications for Early Subduction History of Paleo-Asian Ocean Plate. *Earth Science*, 41(12): 2019–2030

Liu, Y. S., Wang, X. H., Wang, D. B., et al. 2012. Triassic High-Mg Adakitic Andesites from Linxi, Inner Mongolia: Insights into the Fate of the Paleo-Asian Ocean Crust and Fossil Slab-Derived Melt-peridotite Interaction. *Chem*. *Geol*., 328(11): 89–108

Ma, L., Wang, Q., Wyman, D. A., et al., 2015. Late Cretaceous Back-Arc Extension and Arc Systeme Volution in the Gangdese Area, Southern Tibet: Geochronological, Petrological, and Sr-Nd-Hf-O Isotopic Evidence from Dagzedia Bases. *J. Geophys. Res*. *Solid Earth*, 120(9): http://dx.doi:10.1002/2015JB011966.

Melson, W. G., Vallier, T. L.，Wright, T. L., 1976. Chemical Diversity of Abyssal Volcanic Glass Erupted along Pacific, Atlantic and Indian Ocean Sea-Floor Spreading Centers. *Am. Geophys. Union*, *Washington DC*. 351–367

Meschede, M., 1986. A Method of Discriminating between Different Types of Mid-Ocean Ridge Basalts and Continental Tholeiites with the Nb-Zr-Y Diagram. *Chemical Geology*, 56(3–4): 207–218

Miao, L. C., Fan, W. M., Liu, D. Y., et al., 2008. Geochronology and Geochemistry of the Hegenshan Ophiolitic Complex: Implications for Late-Stage Tectonic Evolution of the Inner Mongolia-Daxinganling Orogenic Belt. *Journal of Asian Earth Sciences*, 32(5–6): 348–370

Oyhantcabal, P., Siegesmund, S., Wemmer, K., et al.2007. Post-Collisional Transition from Cale-Alkaline to Alkaline Magmatism during Transcurrent Deformation in the Southernmost Dom Feliciano Belt (Brazilia-no-Pan-Afican,Uruguay). *Lithos*, 98(1–4): 141–159.

Parlak, O., 2016. The Tauride Ophiolites of Anatolia (Turkey): A Review. *Journal of Earth Science*, 27(6): 901–934

Pearce, J. A., 1982. Trace Element Characteristics of Lavas from Destructive Plate Boundaries. In: Thorpe, R. S., ed., Andesites: Orogenic Andesites and Related rocks. *Chichester*: *Wiley*, 525–548

Pearce, J., 2008. Geochemical Fingerprinting of Oceanic Basalts with Applications to Ophiolite Classification and the Search for Archean Oceanic Crust. *Lithos*, 100(1–4): 14–48

Pearce, J. A., Peate, D. W., 1995. Tectonic Implications of the Composition of Volcanic Arc Magmas. Ann. Rev. *Earth Planet. Sci.*, 23: 251–286.

Pearce, J. A., Cann, J. R. 1973. Tectonic Setting of Basic Volcanic Rocks Determined Using Trace Element Analyses. *Earth and Planetary Science Letters*, 19(2): 290–300. doi:10.1146/annurev.ea.23.050195.001343

Pidgeon, R. T., 1996. Zircons: What We Need to Know. *Journal of the Royal Society of Western Australia*, 79 (1): 119–122

Pollock, J. C., Hibbard., J. P., 2010. Geochemistry and Tectonic Significance of the Stony Mountain Gabbro, North Carolina: Implications for the Early Paleozoic Evolution of Carolinia. *Gondwana Research*, 17(2–3): 500–515

Rottura, A., Bargossi, G. M., Caggianelli, A., et al., 1998. Origin and Significance of the Permian High-K Cale-Alkaline Magmatism in the Central-Eastern Southern Alps, Italy. *Lithos*, 45(1–4): 329–348. doi:10.1016/s0024-4937(98)00038-3

Rudnick, R. L., Gao, S., 2003. The Composition of the Continental Crust. In: Holland, H. D., Turekian, K. K., eds., Treatiseon Geochemistry. Oxford, Elsevier. 1–64

Saunders, A. D.,Storey, M., Kent, R. W., et al., 1992. Consequences of Plume-Lithosphere Interactions. In: Storey, B. C., Alabaster, T., Pankhurst, R. J., eds., Magmatism and the Cause of Continental Breakup. *Geol.Soc. Lond. Spec*. *Publ*, 68(1): 41–60

Sengör, A. M. C., Natal'in, B. A., 1996. Paleotectonics of Asia: Fragments of a Synthesis. *World and Regional Geology*, 486–640

Sengör, A. M. C., Natal'in, B. A., Burtman, V. S., 1993. Evolution of the Altaid Tectonic Collage and Paleozoic Crustal Growth in Eurasia. *Nature*. 364(6435): 299–307

Shao, J. A., 1991. Crust Evolution in the Middle Part of the Northern Margin of Sino-Korean Plate. Peking University Press, Beijing. 1–136 (in Chinese with English Abstract)

Shao, J. A., Tang, K. D., He, G. Q., 2014. Early Permian Tectono-Palaeo Geographic Reconstruction of Inner Mongolia, China. *Acta Petrologica Sinica*, 30(7): 1858–1866 (in Chinese with English Abstract)

Shervais, J. W., 1982. Ti-V Plots and the Petrogenesis of Modern and Ophiolitic Lavas. *Earth and Planetary Science Letters*, 59(1): 101–118. doi:10.1016/0012-821x(82)90120-0

Su, Y. Z., 1996. Paleozoic Stratigraphy of Nei Mongol Grass Stratigraphical Pravice. *Jilin Geology*, 15(3–4): 42–54 (in Chinese with English Abstract)

Sun, S. S., McDonough, W. F., 1989. Chemical and Isotope Systematics of

Oceanic Basalts: Implications for Mantle Composition and Process. In: Saunders, A. D., ed., Magmatism in Ocean Basins. G*eological Society Publication*, 42(1): 313–345. doi:10.1144/gsl.sp.1989.042.01.19

Tang, K. D., 1990. Tectonic Development of Paleozoic Fold Belts at the North Margin of the Sino-Korean Craton. *Tectonics*, 9(2): 249–260. doi:10.1029/tc009i002p00249

Tang, K. D., Yan, Z. Y., 1993. Regional Metamorphism and Tectonic Evolution of the Inner Mongolian Suture Zone. *Journal of Metamorphic Geology*, 11(4): 511–513 (in Chinese with English Abstract)

Tang, K. D., Zhang, Y. P., 1991. Tectonic Evolution of Inner Mongolian Suture Zone. In: Xiao, X. C., Tang, Y. Q., eds., Tectonic Evolution of the Southern Margin of the Paleo-Asian Composite Megasuture. Beijing Scientific and Technical House, Beijing. 30–54 (in Chinese with English Abstract)

Tang, W. H., Zhang, Z. C., Li, J. F., et al., 2011. Geochemistry of the Carboniferous Volcanic Rocks of Benbatu Formation in Sonid Youqi, Inner Mongolia and Its Geological Significance. *Acta Scientiarum Naturalium Universitatis Pekinensis*, 47(2): 321–330 (in Chinese with English Abstract)

Wang, Q., Liu, X. Y., Li, J. Y., 1991. Plate Tectonics between Cathaysia and Angaraland in China. Peking University Press, Beijing. 1–151 (in Chinese with English Abstract)

Wilson, M., 1989. Igneous Petrogenesis: A Global Tectonic Approach. Unwin Hyman, London. 1–466

Winchester, J.A., Floyd, P. A., 1977. Geochemical Discrimination of Different Magma Seriesand Their Differentiation Products Using Immobile Elements. *Chemical Geology*, 20(4): 325–343. doi:10.1016/0009-2541(77)90057-2

Windley, B. F., Alexeiev, D., Xiao, W. J., et al., 2007. Tectonic Models for Accretion of the Central Asian Orogenic Belt. *Journal of the Geological Society*, 164(1): 31–47. doi:10.1144/0016-76492006-022

Wood, D. A., 1980. The Application of a Th-Hf-Ta Diagram to Problems of Tectonomagmatic Classification and to Establishing the Nature of Crustal Contamination of Basaltic Lavas of the British Tertiary Volcanic Province. *Earth and Planetary Science Letters*, 50(1): 11–30. doi:10.1016/0012-821x(80)90116-8

Wu, C., Jiang, T., Liu, C. F., et al., 2014. Early Cretaceous A-Type Granites and Momineralization, Aershan Area, Eastern Inner Mongolia, Northeastern China: Geochemical and Isotopic Constraints. *Int. Geol. Rev*. 56(11): 1357–1376. doi:10.1080/00206814.2014.935965

Wu, C., Jiang, T., Liu, W. C., et al., 2015. Early Cretaceous Adakitic Granites and Mineralization of the Yili Porphyry Mo Deposit in the Great Xing'an Range: Implications for the Geodynamic Evolution of Northeastern China. *Int. Geol. Rev*. 57 (9–10): 1152–1171. doi:10.1080/00206814.2014.934746

Wu, Y. B., Zheng, Y. F., 2004. Genesis of Zircon and Its Constraints on Interpretation of U-Pb Age. *Chinese Science Bulletin*, 49(15): 1554–1569 (in Chinese with English Abstract)

Xiao, W. J., Windley, B. F., Hao, J., et al., 2003. Accretion Leading to Collision and the Permian Solonker Suture, Inner Mongolia, China: Termination of the Central Asian Orogenic Belt. *Tectonics*, 22(6): 1069–1089. doi:10.1029/2002tc001484

Xiao, W. J., Shu, L. S., Gao, J., et al., 2008. Continental Dynamics of the Central Asian Orogenic Belt and Its Metallogeny. *Xinjiang Geology*, 26 (1): 4–8 (in Chinese with English Abstract)

Xiao, W. J., Windley, B. F., Huang, B. C., 2009. End-Permian to Mid-Triassic Termination of the Accretionary Processes of the Southern Altaids: Implications for the Geodynamic Evolution, Phanerozoic Continental Growth, and Metallogeny of Central Asia. *International Journal of Earth Science*, 98(6): 1189–1217. doi:10.1007/s00531-008-0407-z

Xiao, W. J., Li, S. Z., Santosh, M., et al., 2012. Orogenic Belts in Central Asia: Correlations and Connections. *J. Asian Earth Sci.*, 49(3): 1–6. doi:10.1016/j.jseaes.2012.03.001

Xiao, W. J., Windley, B. F., Allen, M. B., et al., 2013. Paleozoic Multiple Accretionary and Collisional Tectonics of the Chinese Tianshan Orogenic Collage. *Gondwana Res*., 23(4): 1316–1341. doi:10.1016/j.gr.2012.01.012

Xiao, W. J., Santosh, M., 2014a. The Western Central Asian Orogenic Belt: A Window to Accretionary Orogenesis and Continental Growth. *Gondwana Res*, 25(4): 1429–1444. doi:10.1016/j.gr.2014.01.008

Xiao, W. J., Han, C. M., Liu, W., et al., 2014b. How Many Sutures in the Southern Central Asian Orogenic Belt: Insights from East Xinjiange West Gansu (NW China)? *Geosci. Front.*, 5(4): 525–536. doi:10.1016/j.gsf.2014.04.002

Xiao, W. J., Sun, M., Santosh, M., 2015a. Continental Reconstruction and Metallogeny of the Circum-Junggar Areas and Termination of the Southern Central Asian Orogenic Belt. *Geosci. Front.*, 6(2): 137–140

Xiao W. J., Windley B., Sun, S., et al., 2015b, A Tale of Amalgamation of Three Permo-Triassic Collage Systems in Central Asia: Oroclines, Sutures, and Terminal Accretion. *Annual Review of Earth and Planetary Sciences*, 43(16): 1–31. doi:10.1016/j.gsf.2014.11.003

Xu, B., Chen, B., 1997. The Structure and Evolution of Paleozoic Orogenic Belt between the North China Plate on the Northern Inner Mongolia and Siberian Plate. *Science in China* (*Series D*), 27(3): 227–232 (in Chinese with English Abstract)

Xu, B., Jacques, C., Zhang, F. Q., 2001. Primary Study on Petrology and Geochronology of Blueschists in Sunitezuoqi, Northern Inner Mongolia. *Chinese Journal of Geology*, 4: 424–434 (in Chinese with English Abstract)

Xu, B., Zhao, P., Bao, Q. Z., et al., 2014. Preliminary Study on the Pre-Mesozoic Tectonic Unit Division of the Xing-Meng Orogenic Belt (XMOB). *Acta Petrologica Sinica*, 30(7): 1841–1857 (in Chinese with English Abstract)

Yan, S., Shan, Q., Niu, H. C., et al., 2015. Petrology and Geochemistry of Late Carboniferous Hornblende Gabbro from the Awulale Mountains, Western Tianshan (NW China): Implicationfor an Arc–nascent Back-arc Environment. *Journal of Asian Earth Sciences*, http://dx.doi.org/10.1016/j.jseaes.2015.01.016.

Yarmolyuk, V. V., Kovalenko, V. I., Sal'nikova, E. B., et al., 2008. Geochronology of Igneous Rocks and Formation the Late Paleozoic South Mongolia Active Margin of the Siberian Continent. Stratigraphy and Geological Correlation, 16(2): 162–181. doi:10.1134/s0869593808020056

Zhai, Y. S., 2002. Metallogenics Systems of Paleocontinental Margin. *Geological Publishing House*, Beijing. 1–416 (in Chinese with English Abstract)

Zhang, Q., Qian, Q., Wang, Y., 1999. Geochemical Study on Igneous Rocks of Orogenic Belts. *Earth Science Frontiers*, 6(3): 113–119

Zhu, D. C., Mo, X. X., Wang, L. Q., 2008. Hotspot-Ridge Interaction for the Evolution of Neo-Tethys: Insights from the Late Jurassic-Early Cretaceous Magmatism in Southern Tibet. *Acta Petrological Sinica*, 24(2): 225–237 (in Chinese with English Abstract)

Zhu, Y. Y., Sun, S. H., Mao, Q., 2004. Geochemistry of the Xilingele Complex, Inner Mongolia: A Historic Record from Rodinia Accretion to Continental Collision after Closure of the Paleo-Asian Ocean. *Geological Journal of China Universities*, 10(3): 343–355 (in Chinese with English Abstract)

1 : 50 000 Regional Geological Survey Reports of Balaguer, Alatengguolegongshe, Houtoumiao, Alatengaobaonongdui, Inner Mongolia. 2013. Beijing: China University of Geosciences (in Chinese)